Nuclear Instruments and Methods in Physics Research A 1060 (2024) 169038

Contents lists available at ScienceDirect

Nuclear Inst. and Methods in Physics Research, A

journal homepage: www.elsevier.com/locate/nima

Simulation framework and measurements of crystal collimation of proton beams at the Large Hadron Collider

Rongrong Cai [a,b,*], Roderik Bruce [a], Marco D'Andrea [a], Luigi Salvatore Esposito [a], Pascal Hermes [a], Anton Lechner [a], Daniele Mirarchi [a], Laurence Nevay [a], Jean Baptiste Potoine [a,c], Stefano Redaelli [a], Francesc Salvat Pujol [a], Philippe Schoofs [a], Mike Seidel [b,d]

[a] CERN, Esplanade des Particules 1, Geneva, 1211, Switzerland
[b] École Polytechnique Fédérale de Lausanne, Lausanne, Vaud, Switzerland
[c] University of Montpellier, 163 rue Auguste Broussonnet, Montpellier, 34090, Occitania, France
[d] Paul Scherrer Institut, Forschungsstrasse 111, Villigen, 5232, Aargau, Switzerland

ARTICLE INFO

Keywords:
Crystal channeling
Simulation
LHC
Proton

ABSTRACT

Thanks to its versatility in deploying large kicks with high efficiency, crystal channeling is being integrated more and more into modern particle accelerators. For example, at the CERN Large Hadron Collider, crystals are used, or planned to be used for collimation and fixed-target opportunities for the Physics Beyond Colliders studies. In order to predict and optimize the performance in present and future applications, it is very important to have reliable simulation tools that integrate the crystal effects on the beam with multi-turn tracking. This work shows the setup of a simulation including magnetic tracking, detailed aperture models, particle-matter interactions as well as coherent physics processes in the crystals, using the coupling between SixTrack and FLUKA. A series of simulation tool benchmarks for collimation of multi-TeV protons has been carried out with LHC data.

1. Introduction

The Large Hadron Collider (LHC) [1] at CERN is a particle collider that accelerates and collides two counter-rotating beams of protons or heavy ions, achieving so far energies of up to 6.8 TeV per charge. In recent years, due to their ability in deploying large kicks with high efficiency and potential, Si crystals have been introduced in the LHC. They are able to trap incoming charged particles between or along the crystalline planes and axes thanks to the electromagnetic potential in the regular crystal lattice, while strongly suppressing the inelastic interactions with the crystal nuclei. This mechanism is called crystal channeling (CH) [2] and it occurs when particles enter the crystal with an incident angle below the so-called critical angle, θ_c [3], which is around $2\,\mu\text{rad}$ for LHC energies of 6.5 TeV with a crystal with a bending radius of 80 m. In the LHC, for crystals with this design bending radius, the accumulated angular deviation received is equivalent to a magnetic field of hundreds of Tesla for particles of several TeV. In addition to channeling, other physical processes occur (Table 1): within θ_c there can also be amorphous material interactions (AM) and partial channeling (dechanneling, DC). For larger incoming angles up to the bending angle, particles may be reflected by the crystalline plane (volume reflections, VC) or captured back to channeling (volume capture, VC). Outside the aforementioned ranges, the crystal acts as an amorphous material. Further details about the physics of these processes are found in [2].

One of the most promising usage of crystals in the LHC is for beam collimation, which stems from the need of shielding the machine (especially superconducting magnets) from beam losses that could cause magnet quenches or even damage. For the LHC beam collimation, a multistage system has been deployed [4–7], using amorphous movable collimators with most of them installed in the LHC insertion region 7 (IR7). While the collimation system is used both during proton and heavy-ion operations, due to nuclear fragmentation of ions in the collimators, the collimation system performs worse for ions than for protons [8–10]. With the imminent High-Luminosity LHC (HL-LHC) upgrades [11], the stored Pb beam energy will increase further and a more efficient collimation system is required [12]. Bent crystals are being introduced as a part of the LHC upgrade [13] and will be used as the primary collimation stage to channel halo ions with a reduced fragmentation rate [13–16]. This will give to the ions a coherent angular kick such that they later hit deeply into a downstream standard collimator used as channeled-halo absorber, guaranteeing very small leakage to the superconducting magnets. This method is particularly

* Corresponding author at: CERN, Esplanade des Particules 1, Geneva, 1211, Switzerland.
E-mail address: rongrong.cai@cern.ch (R. Cai).

https://doi.org/10.1016/j.nima.2023.169038
Received 20 October 2023; Received in revised form 11 December 2023; Accepted 19 December 2023
Available online 20 December 2023

Table 1
Table listing the crystal processes linked to the indicative particle incoming angle range. θ_i is the incoming angle, θ_c is the critical angle and θ_b is the bending angle.

Incoming angle	Process
$\theta_i < -\theta_c$	AM
$-\theta_c < \theta_i < \theta_c$	CH, DC, AM, VR
$\theta_c < \theta_i < \theta_b$	VR, Volume capture (VC), AM
$\theta_i > \theta_b$	AM

suitable for ions, as the load on the collimator used as absorber is tolerable. Using the same technique for a full proton beam, where the halo particles can carry up to 1 MW of power, would require a different and more robust absorber design. This is therefore presently not considered.

Although crystal collimation is not used in high-intensity proton runs, they were successfully used to reduce experimental backgrounds in low-intensity special proton runs [17]. Furthermore, collimation tests with low-intensity proton beams allows to gain experience with the operation of a crystal based system and to characterize the installed crystals [18–26]. Currently, there are four crystals installed in the LHC, one per beam and plane. They are of the strip kind, i.e. they use the 110 plane of the Miller index [2] to give an angular deviation to the particles. Historically, quasi-mosaic crystals, i.e. crystals using the 111 plane, have also been used in the LHC [27]. Details for the crystals used during the measurements discussed in this article are shown in Table 2. Note that only 3 out of the present and past crystals were used for the measurements reported here.

Another relevant application of crystals at the LHC is the so-called beam splitting for fixed-target experiments, which is being studied in the CERN initiative of Physics Beyond Colliders (PBC) [28]. The idea is to use the bending produced by the crystal to create precession in the short-lived baryons that are large enough to be measured [29–31]. Beam halo would go through a crystal-target-crystal configuration before they reach the detector. Also for this complex applications, a performing and well-benchmarked simulation framework is required.

Given these applications and their importance, it is crucial to have a simulation tool that integrates the crystal physics processes with particle-matter interactions and multi-turn tracking through an accelerator. Such a tool could be used to investigate operational ideas, quantify expected future performance, find potential performance limitations, and understand experimental results. While the simulations for proton beams are well advanced and succeeded already in predicting accurately various applications [3,17,32,33], the planned heavy-ion collimation requires a multifunctional simulation framework that handles many species of particles. Presently, in conjunction with other collimation activities, the program SixTrack [34] is used to simulate the multi-turn evolution of the beam halo intercepted by a crystal-based collimation system. Detailed information on the physics and benchmark of that code can be found in [3,32,33].

Since the present crystal simulation tool, SixTrack, is limited to protons, an effort was undertaken to expand the simulation toolkit and set up a more general approach, able to handle also heavy ions. Benefiting from the more detailed physics implementation in FLUKA, a new simulation framework that combines accelerator tracking and the coherent crystal interactions has been created. It is built on an existing framework, called SixTrack-FLUKA coupling [35–37], which is the standard tool for simulating ion collimation [9,38]. Here, FLUKA [39,40] is used as the main crystal engine, as well as for generating all other particle-matter interactions. Compared to the analytical approach of SixTrack, FLUKA uses a detailed step-by-step microscopic method within the crystal [41], thus enabling a more realistic tracking. Beside the SixTrack-FLUKA coupling, an effort to include the crystal phenomena in Geant4 and SixTrack is also underway [42,43].

Table 2
Crystal specification of the crystals used in this paper.

Name	Plane	Bending	Length	Width	Height
TCPCH.A4L7	B1H	64.5 µrad	4 mm	2 mm	50 mm
TCPCH.A5R7	B2H	36.4 µrad	4 mm	2 mm	50 mm
TCPCV.A6R7	B2V	51.1 µrad	4 mm	2 mm	50 mm

This paper starts with a description of the simulation framework itself. It is then followed by benchmark results using proton data: single-pass crystal benchmark, loss pattern, angular scan, and linear scan.

2. Simulation framework

The SixTrack-FLUKA coupling [37] provides a framework for active information exchange between SixTrack [34,44] and FLUKA [40,45,46]. SixTrack is a 6D symplectic particle tracking code, whereas FLUKA is a general-purpose Monte Carlo code. SixTrack is used for tracking in the magnetic lattice, while FLUKA simulates particle-matter interactions [35,36].

In recent years, a crystal routine, based on the reduction of certain particle-matter interactions while in channeling, has been developed and integrated in FLUKA [41,47,48]. Building on that, the SixTrack-FLUKA coupling has been updated to enable possibility to integrate crystals as part of the LHC collimation system simulation setup, carrying a special flag and several crystal-specific parameters in the inputs to activate the crystal physics routine. A typical simulation would start with a user defined initial distribution in SixTrack. The particles would be tracked until they reach a collimator, at which point the particle information is exchanged with FLUKA. FLUKA proceeds to simulate the interactions within the collimator and the ones that survive would be sent back to SixTrack. Particles are tracked as long as they are not absorbed or according to a user defined number of turns. Several changes and additions were necessary to accommodate crystal collimators — specific crystal input files, changes to intermediate files responsible for cross-checking between accelerator lattice elements and collimator elements in the FLUKA database (FEDB).

The 3D geometrical models of the crystals in the LHC follow closely the real curved geometries and the crystal lattice properties have been defined according to the X-ray and single-pass measurements with protons of LHC crystals [14], excluding the supporting devices, which do not interfere with the multi-turn dynamics. Since all collimator geometries exist in a FLUKA Elements Database (FEDB), the new crystal collimators have also been added in the database. Therefore, crystal collimators can be included in simulations using the new framework in the same way as other collimators. Finally, crystal-specific output files have been added.

During the development of this framework, a few changes to the crystal routine itself from the FLUKA side have been triggered, e.g. fixes to simulate high-energy particles accurately.

3. Benchmark results

3.1. Single pass

The first type of comparison consists of exploring in detail single-pass studies at high energies (LHC proton energy of 6.5 TeV) independently of multi-turn effects in the accelerator. Comparison has only been done between the simulation tools (SixTrack-FLUKA coupling and the standalone SixTrack routine), as there are no measurements available at this energy for this kind of study [48]. For this purpose, 6×10^6 6.5 TeV protons uniformly distributed in x and x' have been simulated in both codes to hit the crystal face and pass through it only once. The crystal bends in the z–x plane, while the beam travels in the z direction. In order to cover from one amorphous regime to the other for

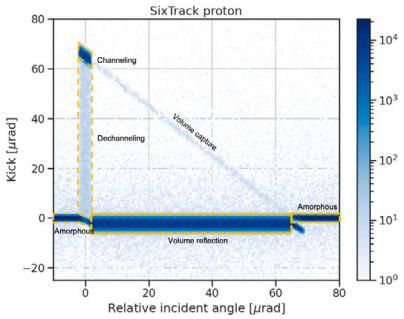

Fig. 1. Simulated proton angular kick distribution as a function of relative angle between incoming particles and crystal orientation with SixTrack after a single pass through the crystal. Protons at 6.5 TeV are considered.

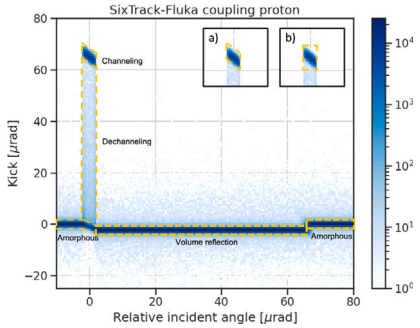

Fig. 2. Simulated proton angular kick distribution as a function of relative angle between incoming particles and crystal orientation with SixTrack-FLUKA coupling after a single pass through the crystal. Proton at 6.5 TeV are considered. Subfigures (a) and (b) compare the final CH boundaries between using small histogram slices – (a) and a rough section cut – (b).

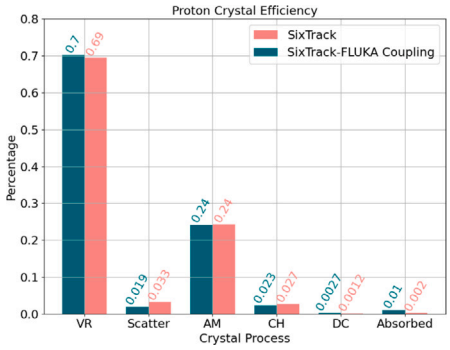

Fig. 3. Crystal interaction process efficiency summary for 6.5 TeV protons with the standalone SixTrack and the SixTrack-FLUKA coupling.

this crystal bending, the distribution extends from 10 μrad to 80 μrad in x' and from −1 mm to 1 mm in x. The crystal used is the TCPCH.A4L7.B1 in Table 2.

The angular kick distribution as a function of impinging angle is shown in Fig. 1 for the standalone SixTrack and in Fig. 2 for the SixTrack-FLUKA coupling. A summary of the channeling efficiency and of the various other coherent and in-coherent phenomena can be found in Fig. 3.

The two tools classify crystal interactions slightly differently. This makes quantitative comparisons difficult. Therefore, crystal interactions have been assigned again independently from the tools, where each particle exiting the crystal has been assigned to a given interaction process (as shown in Table 1) according to its incoming angle and angular kick. The incoming particles are perfectly aligned with the

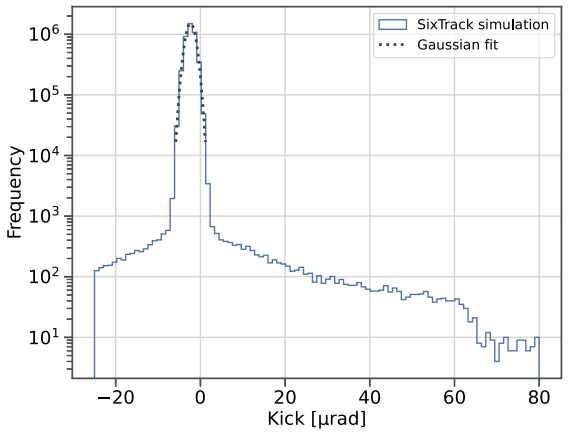

Fig. 4. The blue line is the SixTrack simulated B1H crystal angular kick distribution in VR range with 6.5 TeV protons. The black dashed line is the Gaussian fit of the VR peak. The incoming angle range is from 2 μrad to 65 μrad (as in Table 3).

Table 3
Crystal single pass study incoming angle boundary division for protons. AM: Amorphous; CH: Channeling; DC: Dechanneling; VR: Volume Reflection; VC: volume capture.

SixTrack [μrad]	Coupling [μrad]	Processes
−10 – −2.2	−10 – −2	AM
−2.2 – 2	−2.2 – 2	CH, DC, AM
2 – 65	2 – 66	VR, VC
65 – 80	66 – 80	AM

crystal planes when $\theta_i = 0$. The boundaries of the division in incoming angle can be found in Table 3.

After the division on the horizontal axis, a histogram of received angular kicks for a selected incoming angle window (Figs. 1 and 2) is plotted for each interaction process except for the channeling window. The angular kick distribution is then fitted with a Gaussian function. All particles within the 3 standard deviations are assigned to the process linked to that incoming angle range. An illustration of how the analysis was done is shown in Fig. 4, where the VR region is taken from the incoming angle range of $2\,\mu\text{rad} \leq \theta_i \leq 65\,\mu\text{rad}$ for SixTrack. The left peak corresponds to the VR particles and the right peak to the VC particles. Only the VR peak is being fitted and the occurrences within 3 standard deviations are counted as VR particles, as VC is not included in FLUKA, thus not comparable. The same method is applied to the SixTrack-FLUKA coupling.

For the channeling window, smaller sub-slices of the order of 0.2 to 0.4 μrad in θ_i are taken, because rough rectangular boundaries as the ones shown in Fig. 2 subfigure (b) would include particles that are not fully channeled. Hence, the approach that gives the boundaries in Fig. 2 subfigure (a) is preferred. For each slice, a histogram of angular kicks is plotted and one Gaussian curve is fitted for the channeling region and another for the amorphous region. All particles in between the channeling and amorphous bumps are counted as dechanneled particles. All particles that do not fall within any of the boundaries found are considered scattered particles. Volume captured particles have not been included in the scattered particles, as this process has not yet been included in the FLUKA routine for high energy particles. The difference between the initial and the final number of particles corresponds to the ones absorbed by the crystal.

Overall, Figs. 1 and 2 agree well, despite using different tools. The main differences that can be noticed between the two routines are the lack of volume capture in FLUKA, a different distribution for volume reflection in angular kick (Fig. 5), and a different distribution in incoming angle for the dechanneled particles (Fig. 6). Presently, because there is no experimental single-pass data at this energy, it is not possible to determine the correct approach.

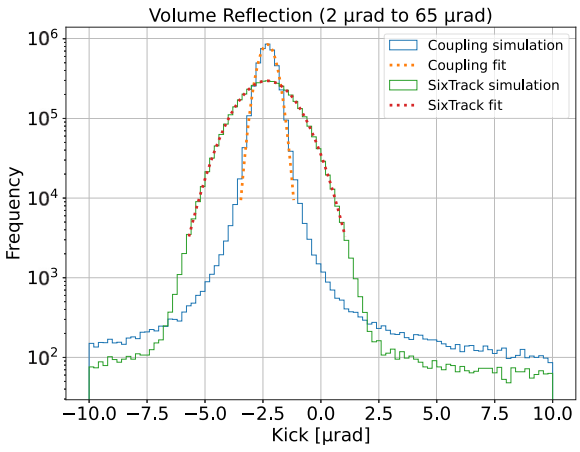

Fig. 5. Comparison of simulated VR distribution in angular kick for the B1H crystal with 6.5 TeV protons. The incoming angle range is $2\,\mu\text{rad} =< \theta_i =< 65\,\mu\text{rad}$. The blue curve is SixTrack-FLUKA coupling simulation and the orange curve the SixTrack simulation, whereas the dashed orange and red lines are their respective Gaussian fits.

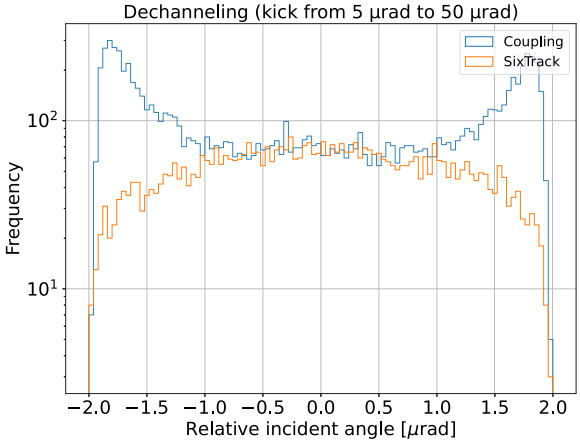

Fig. 6. Comparison of simulated DC in incoming angle for the B1H crystal with 6.5 TeV protons. The range is $-2\,\mu\text{rad} =< \theta_i =< 2\,\mu\text{rad}$ and $-10\,\mu\text{rad} =< \theta_{kick} =< 50\,\mu\text{rad}$. The blue curve is SixTrack-FLUKA coupling and the orange curve SixTrack.

3.2. Simulated loss pattern at the LHC

Having assessed the single-pass crystal treatment of the FLUKA routine, we now assess the crystal as it is inserted in a circular accelerator, which also contains other collimators.

As the purpose of these studies is to improve the LHC collimation performance, one of the methods used to benchmark the multi-turn accuracy of the simulation is the same as used previously for assessing the performance of the standard collimation system [6], quantified by the relative leakage out of the collimators to sensitive elements. Collimation cleaning efficiency is measured by observing the beam loss pattern around the ring during provoked losses, so-called loss maps. Around 4000 beam loss monitors (BLMs) placed around the LHC [49] are used to measure local losses. The measured loss maps are normalized to the instantaneous change in beam intensity, or beam flux of lost particles. The simulation setup is used here to reproduce the measured loss maps with crystals.

As it is computationally intensive to simulate the entire beam including the beam core, which typically does not interact with the collimation system, only the beam halo is simulated. The full diffusion process that brings the halo onto the collimator is also not simulated. Instead, the starting conditions are such that the halo particles have already an amplitude sufficiently large to hit the collimators. The

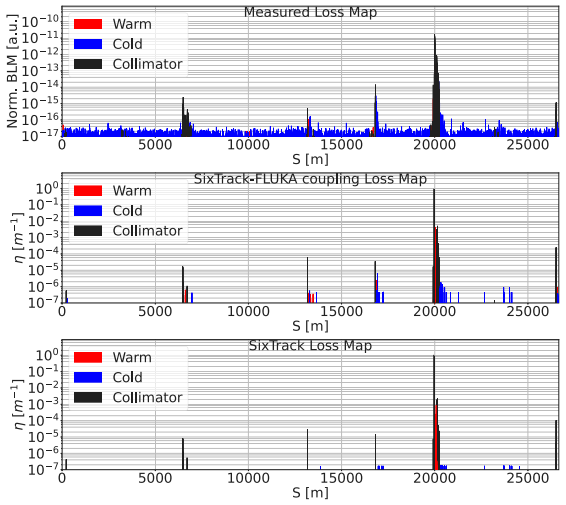

Fig. 7. Measured (top), SixTrack-FLUKA coupling simulated (middle) and SixTrack simulated (bottom) loss map from the B1H 2018 proton test at 6.5 TeV (β^* =1 m).

starting distribution is approximated to a pencil beam at an assumed depth from the collimator edge (impact parameter, b) and generated as in [6]. A pencil beam is a point-like distribution in the phase space. The simulated distribution has 60×10^6 protons and $b = 1\,\mu\text{m}$. This impact parameter is consistent with previous diffusion studies [50–52] but nevertheless carries a large uncertainty. It has a 1 nm spread in x and a 0.1 μrad spread in x'. The impact of variations in the starting distribution is still to be explored in detail. It is very unlikely, though, that the simulation results are strongly dependent on small variations of b. The rest of the set-up closely follows the one used during measurements.

The benchmark case is a LHC B1H loss map with a crystal (specifications in Table 2) in channeling orientation for 6.5 TeV protons, measured on the 12th of September 2018 with a β^* of 1 m and all collimators upstream open. Details of the measurement, along with the optical setup and collimation configurations, can be found in [14]. For simulated loss maps we calculate the local cleaning inefficiency as $\eta(s) = \frac{E(s)}{E_{totql}\Delta s}$, with $E(s)$ being the energy deposited as a function of position s in the ring.

Fig. 7 compares the measured and the simulated loss maps. Black, red, and blue bars represent the losses on the collimators, warm sections and superconducting (cold) sections respectively. The SixTrack-FLUKA coupling shows an excellent agreement with the SixTrack standalone routine, where it should be noted that SixTrack has a higher energy cut (threshold below which a particle is no longer transported) and therefore gives less warm losses around $s = 20150$ m. Above the measurement noise level, a good qualitative agreement of the measured loss pattern with the SixTrack-FLUKA coupling can be observed. A more detailed quantitative comparison is not possible here since the simulations show lost particles and the measurements show the energy deposition at the BLMs from the induced shower. Previous studies have shown that an order-of-magnitude discrepancy can be expected only due to the difference in response of BLMs at different locations [6]. Further discrepancies can be expected from the fact that a single particle loss can cause showers that affect several BLMs. The particle shower propagation to the BLMs is more pronounced in the warm regions, which explains these higher measurement values. With a detailed FLUKA shower propagation simulation, it is also possible to simulate power deposition, such as in [53]. However, this is out of the scope of this paper. Both losses on the IR7 cold magnets and on the rest of the collimators show good agreement, except for a slight underestimation of the simulation compared to data for the collimator cluster around $s = 20100$ m, which may be due to upstream showers. Furthermore, the

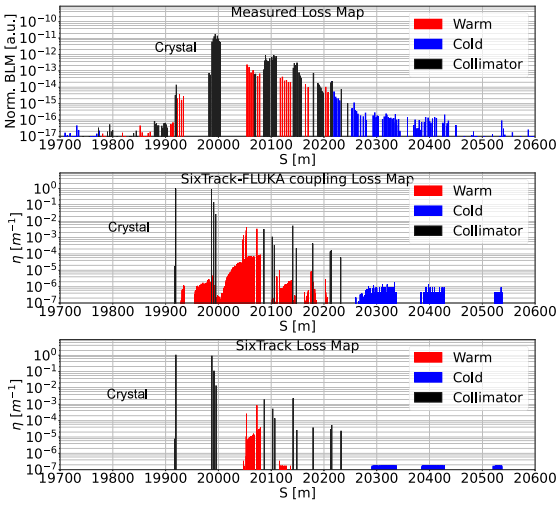

Fig. 8. Measured (top), SixTrack-FLUKA coupling simulated (middle) and SixTrack simulated (bottom) loss map from the 2018 proton test at 6.5 TeV, as in Fig. 7 but zoomed around IR7. The crystal can be found at 19 919.5 m and the absorber at 19 987 m.

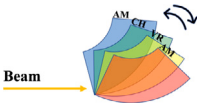

Fig. 9. Angular scan illustration.

high simulated loss at s = 19919.5 m in Fig. 8 representing the crystal cannot be directly compared with the measured data, as the simulation result is normalized to the length of the crystal, which is two orders of magnitude shorter than the other collimators.

Finally, regarding the different treatment of volume processes and dechanneling between the two tools mentioned in the previous paragraph, the accuracy of reproducing the volume processes are not of capital interest to the operations of the LHC, as channeling is the chosen regime. Furthermore, in view of the collimation setup, the doubt on the DC distribution may potentially be a small issue, as long as the downstream absorber has an aperture small enough to capture most of the dechanneled particles that have smaller angular kick together with the CH particles.

3.3. Angular scan

After the multi-turn benchmark with the crystal in the best orientation, we study so-called angular scans that are performed to assess the loss pattern at other crystal orientations. The crystal is rotated with respect to the incoming beam such that the incoming angle changes (a representation is shown in Fig. 9), and the BLM signal close to the crystal is recorded as a function of the angle. The signal at different angles is then normalized by the signal acquired at the orientation where the crystal acts as an amorphous material. The scan ranges over angles where the crystal is in the orientations for channeling, volume reflection, or amorphous scattering, giving rise to variations in the rate of inelastic interactions at the crystal, and hence also the local BLM signal [3].

A comparison of angular scan was made between measured data and the simulation from the two crystal routines. The machine configuration is the one described in Section 3.2 with 6.5 TeV protons in the B1H plane.

The angular scan simulation follows the same method and statistics as loss maps. However, instead of simulating only the case when the crystal is in optimal orientation, other orientations are also simulated

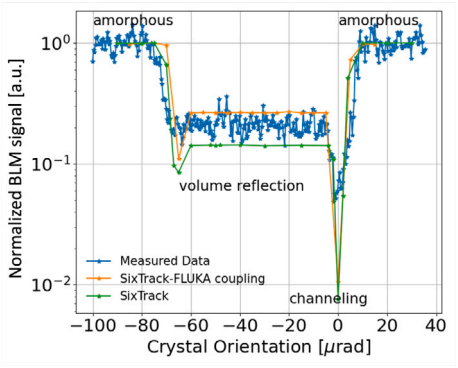

Fig. 10. Measured BLM data from 2018 (blue) [14,21], SixTrack-FLUKA coupling simulation (orange), and SixTrack simulation (green) of the local losses at the TCPCH.A4L7.B1 crystal during an angular scan with 6.5 TeV protons.

and other loss maps created. The crystal orientation stretches from one amorphous orientation to the other as outlined in Table 1. The energy absorbed in the crystal at every orientation is then normalized to the energy absorbed in the amorphous crystal. This is done both for SixTrack and the SixTrack-FLUKA Coupling. The simulation results are compared to the measured data in Fig. 10. The measurement conditions are described more in detail in [21].

A qualitatively good agreement among the three sets of data is observed. The difference in channeling well depth at the sharp minimum with respect to the measured data can in part be explained by imperfections that are not considered in simulation, e.g. changes in impacting angle due to orbit drifts or inherent to the excitation used to create losses. However, in the middle volume reflection section, approximately from −70 μrad to −10 μrad, there seems to be a small underestimation of the measurement by SixTrack and a small overestimation by the SixTrack-FLUKA coupling. This discrepancy, not seen in previous SixTrack studies [27], needs further investigation.

3.4. Linear scan

Lastly, a benchmark using linear scans is performed. In that case, the crystal is kept in channeling orientation, while the absorber is slowly moved towards the beam starting from an open position where it does not intercept the channeled halo (Fig. 11), to gradually intercept it and reconstruct its profile with an error function from the BLM signal. After the absorber has moved beyond the point where it intercepts the entire channeled halo, the BLM signal at the absorber continues to rise slowly, as the absorber approaches the beam, until a spike of high losses occurs at the beam core boundary. This slow rise prior to this point is caused by intercepting particles that are dechanneled at smaller angular kicks or see the crystal as an amorphous material.

Linear scans are used to estimate experimentally the multi-turn channeling efficiency and the bending angle of the crystal. The multi-turn channeling efficiency is defined as N_{CH}/N_{tot}, where N_{CH} is the number of particles channeled over all the turns the particles remain circulating and N_{tot} is the total number of the particles impacting on the crystal at the first turn. The ratio between the theoretical plateau level of the error function and the level before the absorber attains the beam core represents the multi-turn channeling efficiency, while the inflection point of the error function gives the bending angle.

The data taken come from the 2022 machine development B2V crystal tests with 6.8 TeV protons. The optics and collimation settings can be found in [54,55]. The experimental data are normalized to the beam loss rate and to the level of the BLM signal just before the absorber intercepts the core (occurring with the absorber at the same σ aperture as the crystal), as it gives the intensity of the entire beam halo that impacted the crystal.

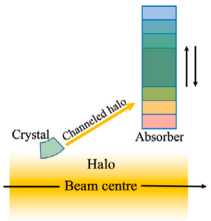

Fig. 11. Linear scan illustration.

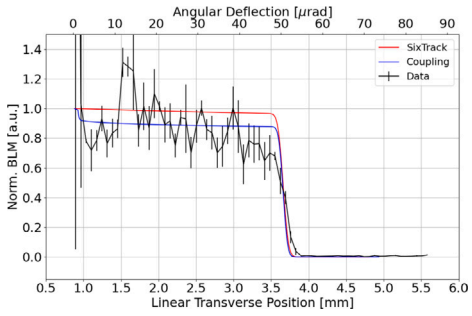

Fig. 12. Measured (black) and simulated (SixTrack — red, SixTrack-FLUKA Coupling — blue) B2V crystal linear scan for 6.8 TeV proton.

To simulate this case, a pencil beam with 3×10^5 protons and 1 μm impact parameter on the crystal was used. The absorber has been closed to the same σ aperture of the crystal (5.2 σ), and the distribution of the particles on the absorber has been recorded. The particle distribution on the vertical axis is then integrated from the open position of the collimator ($+\infty$) to all intermediate points and normalized to the total number of protons impacting the crystal. The results are shown in Fig. 12.

The simulated results show a reasonable reproduction of the BLM signal, considering that the sustained loss rate of the beam over time is noisy and that we are simulating a perfect machine. The SixTrack-FLUKA Coupling gives a multi-turn efficiency of approximately 87%, which is a closer reproduction of the measured one at around 70%±15%, whereas, for SixTrack's simulation, this is almost 10% higher. The differences from the two tools may come from the different scattering treatment [39,56,57], given the satisfactory agreement seen in Fig. 3.

4. Conclusion

A simulation framework that is based on the existing coupling between the magnetic tracking in SixTrack and particle-matter interaction in FLUKA has been built for crystal studies in particle accelerators. With the inclusion of coherent effects from bent crystals on the beam in the SixTrack-FLUKA Coupling, using the step-by-step microscopic FLUKA model of crystal interactions, the new framework can treat different particle types in a general way, as opposed to previous multi-turn tools, in particular the built-in SixTrack routine, that can handle protons only. On the other hand, the SixTrack framework has been extensively benchmarked against measurement data from different machines and, for proton beam, it represents the present state-of-the-art for multi-turn crystal simulation processes. The new simulation setup has thus been benchmarked with the built-in routine in SixTrack for protons, and with high-energy 6.5 TeV proton data from the LHC. Benchmark studies include single-turn and multi-turn studies. For multi-turn studies, the focus has been put on beam collimation usages, such as particle loss patterns. Crystal characterization studies, such as angular and linear scans, have also been benchmarked.

Overall, all the benchmark results are satisfactory and no striking discrepancies with measured data were found. It is concluded that the new framework is thus suitable for extensive usage for protons in the investigated parameter range. Minor differences have been identified between the SixTrack-FLUKA Coupling and the standalone SixTrack routine. However, these differences are difficult to explore since there are little or no experimental data at this energy and precision. For future studies, these differences may be explored further, e.g. by using single-pass measurements at lower beam energies. In particular, a benchmark with experimental data should be done for other particle species, especially heavy ions, for which crystal collimation will be used in future physics runs at the LHC. For this application, it is crucial to have a working simulation code, and the presented simulation framework provides a very important step towards that direction.

Declaration of competing interest

The authors declare that they have no known competing financial interests or personal relationships that could have appeared to influence the work reported in this paper.

References

[1] O.S. Brüning, et al., LHC Design Report V.1 : The LHC Main Ring, CERN-2004-003-V1, CERN, Geneva, Switzerland, 2004, CERN, Geneva, Switzerland.
[2] V.M. Biryukov, Y.A. Chesnokov, V.I. Kotov, Crystal Channeling and Its Application At High-Energy Accelerators, 1997.
[3] D. Mirarchi, Crystal Collimation for LHC (Ph.D. thesis), Imperial College, London, 2015, URL http://cds.cern.ch/record/2036210.
[4] R.W. Assmann, Collimators and beam absorbers for cleaning and machine protection, in: Proceedings of the LHC Project Workshop - Chamonix XIV, Chamonix, France, 2005, p. 261.
[5] R.W. Assmann, et al., The final collimation system for the LHC, in: Proc. of the European Particle Accelerator Conference 2006, Edinburgh, Scotland, 2006, p. 986.
[6] R. Bruce, et al., Simulations and measurements of beam loss patterns at the CERN large hadron collider, Phys. Rev. ST Accel. Beams 17 (2014) 081004, http://dx.doi.org/10.1103/PhysRevSTAB.17.081004, URL http://link.aps.org/doi/10.1103/PhysRevSTAB.17.081004.
[7] R. Bruce, et al., Reaching record-low β^* at the CERN large hadron collider using a novel scheme of collimator settings and optics, Nucl. Instrum. Methods Phys. Res. A 848 (2017) 19–30, http://dx.doi.org/10.1016/j.nima.2016.12.039, URL http://www.sciencedirect.com/science/article/pii/S0168900216313092.
[8] P. Hermes, et al., Measured and simulated heavy-ion beam loss patterns at the CERN large hadron collider, Nucl. Instrum. Methods Phys. Res. A 819 (2016) 73–83, http://dx.doi.org/10.1016/j.nima.2016.02.050, URL https://www.sciencedirect.com/science/article/pii/S0168900216002175?via%3Dihub.
[9] N. Fuster-Martínez, et al., Simulations of heavy-ion halo collimation at the CERN large hadron collider: Benchmark with measurements and cleaning performance evaluation, Phys. Rev. Accel. Beams 23 (2020) 111002, http://dx.doi.org/10.1103/PhysRevAccelBeams.23.111002, URL https://link.aps.org/doi/10.1103/PhysRevAccelBeams.23.111002.
[10] N.F. Martinez, et al., Run 2 collimation overview, in: Proceedings of the 9th LHC Operations Evian Workshop, Evian, France, 2019, URL http://cds.cern.ch/record/2750291?ln=en.
[11] I.B. Alonso, et al., High-luminosity large hadron collider (HL-LHC): Technical design report, in: CERN Yellow Reports: Monographs, CERN-2020-0010, CERN, Geneva, 2020, http://dx.doi.org/10.23731/CYRM-2020-0010, URL http://cds.cern.ch/record/2749422?ln=en.
[12] R. Bruce, M. Jebramcik, J. Jowett, T. Mertens, M. Schaumann, Performance and luminosity models for heavy-ion operation at the CERN Large Hadron Collider, Eur. Phys. J. Plus 136 (2021) 745, http://dx.doi.org/10.1140/epjp/s13360-021-01685-5.
[13] S. Redaelli, R. Bruce, A. Lechner, A. Mereghetti, Chapter 5: Collimation system, in: I. Béjar Alonso, O. Brüning, P. Fessia, L. Rossi, L. Tavian, M. Zerlauth (Eds.), CERN Yellow Rep. Monogr. 10 (2020) 87–114, http://dx.doi.org/10.23731/CYRM-2020-0010.87.
[14] M. D'Andrea, Applications of Crystal Collimation to the CERN Large Hadron Collider (LHC) and its High Luminosity Upgrade Project (HL-LHC) (Ph.D. thesis), University of Padova, 2021, URL http://cds.cern.ch/record/2758839, Presented 23 Feb 2021.
[15] W. Scandale, A. Kovalenko, A. Taratin, Experiments with crystal deflectors for high energy ion beams: Electromagnetic dissociation probability for well channeled ions, Phys. Rev. Spec. Top. Accel. Beams 16 (2013) 011001, http://dx.doi.org/10.1103/PhysRevSTAB.16.011001, URL https://cds.cern.ch/record/1709374.

[16] U. Uggerhø j, H. Hansen, K. Jessen, H. Knudsen, E. Uggerhoj, C. Scheidenberger, C. Biino, M. Clement, N. Doble, K. Elsener, L. Gatignon, P. Grafstrom, P. Sona, A. Mangiarotti, S. Ballestrero, Strong suppression of nuclear-charge changing interactions for 18 TeV/c In ions channeled through a bent Si crystal, Phys. Lett. B 619 (2005) 240–246, http://dx.doi.org/10.1016/j.physletb.2005.06.003.

[17] D. Mirarchi, et al., Reducing beam-related background on forward physics detectors using crystal collimation at the large hadron Collider1, Phys. Rev. Appl. 14 (2020) 064066, http://dx.doi.org/10.1103/PhysRevApplied.14.064066, URL https://link.aps.org/doi/10.1103/PhysRevApplied.14.064066.

[18] M. D'Andrea, et al., Crystal collimation performance at the LHC with a 6.8 TeV proton beam, in: Proceedings of the International Particle Accelerator Conference 2023, Venice, Italy, 2023.

[19] M. D'Andrea, et al., First experience of crystal collimators during LHC special runs and plans for the future, in: Proceedings of the 64th ICFA Advanced Beam Dynamics Workshop on High-Intensity and High-Brightness Hadron Beams, Vol. HB2021, 2022, p. MOCC3, http://dx.doi.org/10.18429/JACoW-HB2021-MOCC3.

[20] M. D'Andrea, et al., Crystal collimation tests with proton beams, 2019, URL https://cds.cern.ch/record/2678779.

[21] M. D'Andrea, et al., Operational aspects of crystal collimation with proton beams, 2019, URL https://cds.cern.ch/record/2678780.

[22] R. Rossi, et al., Crystal collimation cleaning measurements with proton beams in LHC, 2016, URL https://cds.cern.ch/record/2306605.

[23] R. Rossi, et al., Beam 2 crystal characterization measurements with proton beams in the LHC, 2018, URL https://cds.cern.ch/record/2643353.

[24] R. Rossi, et al., Crystal Collimation with Protons at Injection Energy, CERN-ACC-NOTE-2016-0035, 2016.

[25] R. Rossi, et al., Crystal collimation with protons at flat top energy, 2017, URL https://cds.cern.ch/record/2257957.

[26] W. Scandale, et al., Observation of channeling for 6500 gev/c protons in the crystal assisted collimation setup for LHC, Phys. Lett. B 758 (2016) 129–133, http://dx.doi.org/10.1016/j.physletb.2016.05.004, URL http://www.sciencedirect.com/science/article/pii/S0370269316301514.

[27] R. Rossi, Experimental Assessment of Crystal Collimation at the Large Hadron Collider (Ph.D. thesis), 2017, Presented 26 Jan 2018, URL https://cds.cern.ch/record/2644175.

[28] J. Beacham, et al., Physics beyond colliders at CERN: beyond the standard model working group report, J. Phys. G: Nucl. Part. Phys. 47 (1) (2019) 010501, http://dx.doi.org/10.1088/1361-6471/ab4cd2.

[29] K. Dewhurst, D. Mirarchi, M. D'Andrea, P. Hermes, S. Redaelli, Performance of a double-crystal setup for LHC fixed-target experiments, in: Proceedings of the International Particle Accelerator Conference 2023, Venice, Italy, 2023.

[30] A.S. Fomin, et al., Feasibility of measuring the magnetic dipole moments of the charm baryons at the LHC using bent crystals, J. High Energy Phys. 2017 (8) (2017) 120(1–27), http://dx.doi.org/10.1007/JHEP08(2017)120.

[31] D. Mirarchi, A. Fomin, S. Redaelli, W. Scandale, Layouts for fixed-target experiments and dipole moment measurements of short-lived baryons using bent crystals at the LHC, Eur. Phys. J. C 80 (10) (2020) 1–16.

[32] D. Mirarchi, G. Hall, S. Redaelli, W. Scandale, A crystal routine for collimation studies in circular proton accelerators, Nucl. Instrum. Methods Phys. Res. B 355 (2015) 378–382. 5 p, http://dx.doi.org/10.1016/j.nimb.2015.03.026, URL https://cds.cern.ch/record/2159102.

[33] D. Mirarchi, S. Redaelli, W. Scandale, Crystal implementation in SixTrack for proton beams, in: Proc. of the ICFA Mini-Workshop on Tracking for Collimation, 2018, pp. 91–108, http://dx.doi.org/10.23732/CYRCP-2018-002.91, URL https://cds.cern.ch/record/2694336.

[34] R. De Maria, et al., SixTrack version 5: Status and new developments, in: Proc. IPAC'19, JACoW Publishing, Geneva, Switzerland, pp. 3200–3203, http://dx.doi.org/10.18429/JACoW-IPAC2019-WEPTS043, URL http://accelconf.web.cern.ch/ipac2019/papers/WEPTS043.pdf.

[35] P.D. Hermes, et al., Simulation of heavy-ion beam losses with the SixTrack-FLUKA active coupling, in: Proc. IPAC'16, JACoW Publishing, Geneva, Switzerland, pp. 2490–2493, http://dx.doi.org/10.18429/JACoW-IPAC2016-WEPMW029, URL https://jacow.org/ipac2016/papers/WEPMW029.pdf.

[36] A. Mereghetti, et al., SixTrack-Fluka active coupling for the upgrade of the SPS scrapers, in: Proc. IPAC'13, JACoW Publishing, Geneva, Switzerland, pp. 2657–2659, URL https://jacow.org/IPAC2013/papers/WEPEA064.pdf.

[37] E. Skordis, et al., FLUKA coupling to sixtrack, in: Proc. of the ICFA Mini-Workshop on Tracking for Collimation, 2018, pp. 17–25, http://dx.doi.org/10.23732/CYRCP-2018-002.17, URL https://cds.cern.ch/record/2694313.

[38] P. Hermes, Heavy-Ion Collimation at the Large Hadron Collider : Simulations and Measurements (Ph.D. thesis), University of Munster, 2016.

[39] C. Ahdida, et al., New capabilities of the FLUKA multi-purpose code, Front. Phys. 9 (2022) 788253, http://dx.doi.org/10.3389/fphy.2021.788253.

[40] G. Battistoni, et al., Overview of the FLUKA code, Ann. Nucl. Energy 82 (2015) 10–18, http://dx.doi.org/10.1016/j.anucene.2014.11.007.

[41] P. Schoofs, Monte Carlo Modeling of Crystal Channeling at High Energies (Ph.D. thesis), EPFL Lausanne, 2014, Presented 18 Mar 2014, URL https://cds.cern.ch/record/1950908.

[42] L. Nevay, Status of crystal simulations with the Geant4 routine, 2020, Presentation at the LHC Collimation Upgrade Specification Meeting, CERN, Geneva, Switzerland.

[43] L. Nevay, et al., BDSIM: Recent developments and new features beyond V1.0, in: 10th International Particle Accelerator Conference, JACoW Publishing, 2019, pp. 1–4, http://dx.doi.org/10.18429/JACoW-IPAC2019-WEPTS058.

[44] R. De Maria, A. Mereghetti, J. Molson, K. Sjobak, SixTrack status, in: Proc. of the ICFA Mini-Workshop on Tracking for Collimation, 2018, pp. 11–15, http://dx.doi.org/10.23732/CYRCP-2018-002.11, URL https://cds.cern.ch/record/2694311.

[45] C. Ahdida, et al., New capabilities of the FLUKA multi-purpose code, Front. Phys. 9 (2022) http://dx.doi.org/10.3389/fphy.2021.788253, URL https://www.frontiersin.org/article/10.3389/fphy.2021.788253.

[46] S. Roesler, R. Engel, J. Ranft, The Monte Carlo Event Generator DPMJET-III, SLAC Report SLAC-PUB-8740, 2000.

[47] P. Schoofs, F. Cerutti, A. Ferrari, G. Smirnov, Monte Carlo modeling of crystal channeling at high energies, Nucl. Instrum. Methods Phys. Res. B 309 (2013) 115–119, http://dx.doi.org/10.1016/j.nimb.2013.02.027, The 5th International Conference "Channeling 2012", "Charged & Neutral Particles Channeling Phenomena" September 23-28, 2012, Alghero (Sardinia), Italy, URL https://www.sciencedirect.com/science/article/pii/S0168583X1300284X.

[48] P. Schoofs, F. Cerutti, A. Ferrari, G. Smirnov, Benchmark of the FLUKA model of crystal channeling against the UA9-H8 experiment, Nucl. Instrum. Methods Phys. Res. B 355 (2015) 374–377, http://dx.doi.org/10.1016/j.nimb.2015.03.074, Proceedings of the 6th International Conference Channeling 2014: "Charged & Neutral Particles Channeling Phenomena" October 5-10, 2014, Capri, Italy, URL https://www.sciencedirect.com/science/article/pii/S0168583X15003092.

[49] E.B. Holzer, et al., Development, production and testing of 4500 beam loss monitors, in: Proc. of the European Particle Accelerator Conf. 2008, Genoa, Italy, 2008, p. 1134.

[50] R. Assmann, F. Schmidt, F. Zimmermann, Equilibrium beam distribution and halo in the LHC, in: Proc. of the European Particle Accelerator Conf. 2002, Paris, France, 2002, p. 1326, URL http://accelconf.web.cern.ch/e02/PAPERS/WEPLE048.pdf.

[51] A. Gorzawski, et al., Probing LHC halo dynamics using collimator loss rates at 6.5 TeV, Phys. Rev. ST Accel. Beams 23 (2020) 044802.

[52] G. Valentino, et al., Beam diffusion measurements using collimator scans in the LHC, Phys. Rev. ST Accel. Beams 16 (2013) 021003, http://dx.doi.org/10.1103/PhysRevSTAB.16.021003.

[53] J.B. Potoine, et al., Power deposition studies for standard and crystal-assisted heavy ion collimation in the CERN large hadron collider, Phys. Rev. Accel. Beams 26 (2023) 093001, http://dx.doi.org/10.1103/PhysRevAccelBeams.26.093001, URL https://link.aps.org/doi/10.1103/PhysRevAccelBeams.26.093001.

[54] S. Fartoukh, et al., LHC Configuration and Operational Scenario for Run 3, CERN-ACC-2021-0007, URL http://cds.cern.ch/record/2790409.

[55] D. Mirarchi, R. Bruce, S. Redaelli, M.S. Camillocci, F.V.D. Veken, Review of operational cycles and their collimator settings, 2022, Presentation at the 31st ABP-NDC section meeting, CERN, Geneva, Switzerland, URL https://indico.cern.ch/event/1148933/contributions/4821135/attachments/2436971/4186879/ReviewOPcycles_DM.pdf.

[56] J. Molson, Proton scattering and collimation for the LHC and LHC luminosity upgrade (Ph.D. thesis), University of Manchester, 2014, URL https://www.research.manchester.ac.uk/portal/en/theses/proton-scattering-and-collimation-for-the-lhc-and-lhc-luminosity-upgrade(3c4fab61-2d9d-4575-8874-15d91c95523f).html.

[57] N.C. Lasheras, Transverse and Longitudinal Beam Collimation in a High-Energy Proton Collider (LHC) (Ph.D. thesis), University of Zaragoza, 1998.